Fiber in-line Mach–Zehnder interferometer fabricated by femtosecond laser micromachining for refractive index measurement with high sensitivity

Ying Wang,[1,2] Minwei Yang,[1] D. N. Wang,[1,*] Shujing Liu,[1] and Peixiang Lu[1,2]

[1]*Department of Electrical Engineering, The Hong Kong Polytechnic University, Hung Hom, Kowloon, Hong Kong, China*

[2]*Wuhan National Laboratory for Optoelectronics, Huazhong University of Science and Technology, Wuhan 430074, China*

**Corresponding author: eednwang@polyu.edu.hk*

Received September 15, 2009; revised December 11, 2009; accepted December 21, 2009; posted December 23, 2009 (Doc. ID 117078); published February 2, 2010

We report a compact fiber in-line Mach–Zehnder interferometer for refractive index sensing with high sensitivity and precise sensing location. One arm of the interferometer contains a microcavity formed by removing part of the fiber core near the core and cladding interface by femtosecond laser micromachining, and the other arm remains in line with the remaining part of the fiber core. Such a fiber in-line Mach-Zehnder interferometer exhibits an extremely high refractive-index-sensitivity of –9370 nm/RIU (refractive index unit) within the refractive index range between 1.31 and 1.335. © 2010 Optical Society of America

OCIS codes: 060.2370, 320.7140, 230.1150.

1. INTRODUCTION

Refractive index sensors based on optical fiber have attracted increasing attention in research owing to their applications in chemical, biomedical, and environmental monitoring. An optical fiber refractive index sensor can be realized by various schemes such as employing fiber Bragg grating [1–3], long-period fiber grating [4–6], interferometer [7,8], and other interesting configurations [9,10]. In many cases, a fiber in-line Mach–Zehnder interferometer (MZI) is of great interest because of its simplicity, compactness, and relatively simple fabrication and signal detection [10–16]. Various types of fiber in-line MZI structures have been developed, including a long-period grating pair [11–13], and a tapered structure has been introduced in both a conventional single-mode fiber (SMF) and in a photonic crystal fiber (PCF) [10,14–16]. However, such MZIs are based on interference between the fundamental core mode and the higher-order cladding mode, with size of typically in the order of millimeters or centimeters, and have very small effective refractive index (RI) difference between the core mode and the cladding mode (<0.01). This essentially limits their applications in some cases where RI variation needs to be precisely located.

Recently, C. Grillet and P. Domachuk *et al.* have proposed a compact single-beam microfluidic MZI of which the optical path difference (OPD) is achieved through light propagation across a fluid–air interface [17–19]. This type of MZI exhibits high compactness and tunability and shows an extinction ratio of over 25 dB. However, the configuration they proposed contains three individual elements, with two sections of SMF functioning as light launching and output port, respectively, and one liquid-filled capillary producing the OPD required, thus additional precise alignment is needed. The integration of these individual elements would be advantageous, which could be achieved in a single fiber by the use of femtosecond laser micromachining.

The femtosecond laser is an efficient tool for many in-fiber optical device fabrications because of its fast and highly accurate material processing capability. By the use of femtosecond laser, a number of microchannel and/or microhole and Fabry–Perot interferometers (FPIs) have been fabricated in the fiber and used for RI sensing [20–23].

In this paper, we present a compact structure of fiber in-line MZI fabricated by femtosecond laser micromachining. One of the interferometer arms contains a microcavity created by removing part of the fiber core near the core and cladding interface, and the other arm lies in the remaining part of the fiber core. The interferometer exhibits a high RI sensitivity, ~–9370 nm/RIU within the RI range between 1.31 and 1.335. Moreover, a precise sensing location can be ensured owing to the small size of the interferometer.

2. MZI FABRICATION AND OPERATION PRINCIPLE

Figure 1 shows the experimental setup for MZI fabrication. In the fabrication process, the femtosecond laser pulses ($\lambda=800$ nm) with the duration of 120 fs and the repetition rate of 1 kHz were focused onto the fiber by a 10× objective lens with a NA value of 0.25 and a working distance of 7 mm. The group-velocity dispersion in the op-

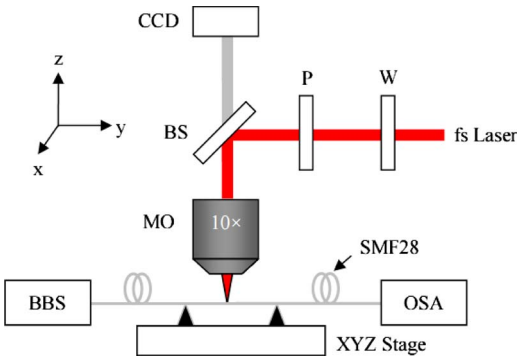

Fig. 1. (Color online) Experimental setup. CCD, charge-coupled device camera; W, half-wave plate; P, polarizer; BS, beam splitter; MO, microscopic objective; BBS, broadband light source; OSA, optical spectrum analyzer; XYZ Stage, computer-controlled three-dimensional translation stage.

tical system was minimized by the adjustment of the amplifier of the laser system. The pulse energy was adjustable in the range between 0 and 1 mJ by rotating the half-wave plate (incorporated with the polarizer), and the average on-target laser power was maintained at ~12 mW. The fiber used was a standard SMF-28 (from Corning) with the core diameter of 8.2 μm and the nominal effective index of 1.4682 (@1550 nm). The fiber was mounted on a computer-controlled three-axis (*XYZ*) translation stage of 40-nm resolution, in parallel with the *Y* axis. The laser focal spot was located at the center of the fiber core, along the *Y* axis. During the fabrication process, the fiber was shifted by 20 μm away from the *Y* axis, and this position was set to be the jumping-off point. The microcavity of the fiber MZI was created by direct femtosecond laser pulse ablation, scanning in parallel with the Y-axis at a speed of 20 μm/s, with the scanning distance of 40 μm and then returned to the starting point. This formed one scanning cycle. A CCD camera was used to monitor the micromachining process and the morphology of the cavity. A broadband light source and an optical spectrum analyzer (OSA) with the resolution of 0.01 nm were connected to the fiber to observe the transmission spectra in real time. After each scanning cycle, the focal point of the laser beam was moved towards to the fiber core along the *X* axis with a step of 400 nm before the next cycle started, until the expected transmission spectrum was obtained. The microcavity created was cleaned with methanol after the processing was completed.

The schematic structure, the optical microscopic image, and the scanning electron microscope (SEM) image of the single-fiber MZI device are shown in Fig. 2. It can be seen from Fig. 2(a) that a MZI cavity is formed by removing part of the fiber core near the core and cladding interface, which results in splitting of the input beam into two portions, denoted by I_{in1} and I_{in2}, respectively. While I_{in1} remains traveling along the fiber core, I_{in2} has to propagate through the microcavity, and the interference happens when the two output beams, I_{out1} and I_{out2}, corresponding to I_{in1} and I_{in2}, respectively, recombine at the fiber core. Because of the low reflectivity at the laser-ablated cavity surface, the multiple reflections of the cavity can be neglected, and thus the MZI device can be characterized by the well-known two-beam optical interference equation as

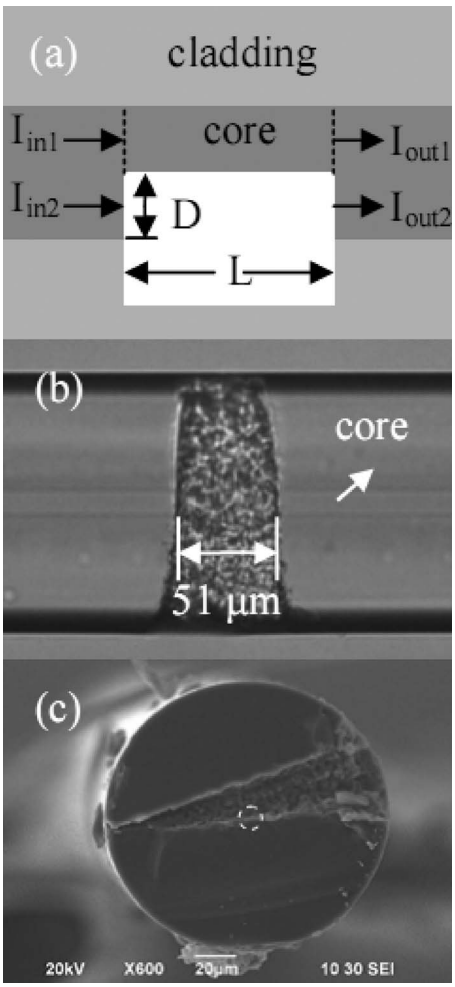

Fig. 2. In-line fiber MZI fabricated by use of femtosecond laser pulse irradiation. (a) Schematic of the structure (top view). D represents the removed size of fiber core; L is the cavity length; I_{inm} and I_{outm} ($m=1,2$) are the input and output optical intensities propagated in the fiber core and microcavity, respectively. (b) Optical microscopic image of the microcavity (side view). (c) SEM image of the microcavity; the dashed white circle indicates the fiber core (cross-section view).

$$I = I_{\text{out1}} + I_{\text{out2}} + 2\sqrt{I_{\text{out1}} I_{\text{out2}}} \cos\left(\frac{2\pi L \Delta n}{\lambda} + \varphi_0\right), \quad (1)$$

where I represents the intensity of the interference signal, λ is the wavelength, and φ_0 is the initial phase of the interference. $\Delta n = n_{\text{eff}} - n_{\text{cavity}}$ denotes the effective index difference of the two interferometer arms within the cavity, where n_{eff} and n_{cavity} are the effective RI of the core and that of the cavity mode, respectively. According to Eq. (1), the interference signal reaches its minimum when the following condition is satisfied:

$$\frac{2\pi L \Delta n}{\lambda_m} + \varphi_0 = (2m+1)\pi, \quad (2)$$

where m is an integer and λ_m is the central wavelength of the mth order interference dip.

3. EXPERIMENTAL RESULTS AND DISCUSSION

In Fig. 2(a), D represents the maximum size of the removed fiber core, which is the key parameter that can be controlled to obtain the optimal fringe visibility of the interference. According to the optical microscopic image as shown in Fig. 2(b), the cavity length of the MZI device, L, is measured to be ~51 μm. The removed size of the fiber core could be estimated as D=4.4 μm according to the SEM image of the cavity cross-section demonstrated in Fig 2(c). The relatively large surface roughness implies that the laser power used was somewhat too high. A better surface quality could be achieved by optimizing the processing parameters such as pulse energy and scanning speed [23].

The output spectrum of the in-line fiber MZI with an air cavity presented in Fig. 2(b) at room temperature was recorded in Fig. 3(a) (dotted black curve), where an insertion loss of ~14 dB and the fringe visibility of ~4 dB can be observed. The relatively large insertion loss was mainly attributed to two reasons: (1) the scattering loss at the cavity border, where the surface roughness is on the order of a micron, (2) the loss of the unguided mode propagated in the cavity. By carefully controlling the laser processing power and scanning speed, the surface roughness and hence the insertion loss may be decreased, however, the unguided mode created loss might not be eliminated. The insertion loss of the device can also be decreased when immersed into the RI liquids, probably due to the reduced RI difference at the cavity surface, which will suppress the scattering loss.

The fringe visibility depends on three factors: (1) the size of the removed fiber core, i.e., D, (2) the loss of the unguided mode in the cavity, (3) the absorption of the cavity medium. D determines the relative intensity of I_{in1} and I_{in2}, and the latter two factors determine the values of I_{out1} and I_{out2}. The highest fringe visibility appears when $I_{out1}=I_{out2}$. It turns out that an MZI device with the highest fringe visibility in air ($n_{cavity}=1$) would exhibit a degraded fringe visibility in RI liquids due to the reduction of the RI difference, Δn, which causes the decrease of the unguided mode loss and the interface scattering loss, without considering the liquid-absorption loss. Assuming that the optimum visibility for the MZI is initially achieved in air, when the device is immersed into the RI liquids, the value of D should be reduced to maintain optimum visibility. On the other hand, if optimum visibility is achieved for the MZI immersed in the RI liquids, then such cannot be maintained for the device in air. This explains why the 51-μm cavity exhibits ~4 dB fringe visibility in air ($n_{cavity}=1$) while ~9 dB in RI liquids ($n_{cavity}\approx 1.3$).

To test the system response to the RI change, the in-line fiber MZI structure was immersed into a series of RI liquids (from Cargille Laboratories) in the RI range of 1.305–1.340 (@489.3 nm) with an interval of 0.005, and the transmission spectra recorded had a resolution of 0.1 nm. Each time after the liquid sample was measured, the fiber device was rinsed with methanol carefully until the original spectrum (i.e., the reference spectrum) could be restored and no residue liquid was left inside the microcavity. The typical transmission spectra of the MZI device corresponding to the RI values of 1.31, 1.32, and 1.33 were plotted in Fig. 3(a). The spectrum of 1.31 RI liquid exhibited two resonance wavelengths of 1314.87 and 1584.47 nm in the wavelength region of 1275–1650 nm, and the free spectral range (FSR) could be determined as ~270 nm. The wavelength shift corresponding to different RI values between 1.31 and 1.335 were demonstrated in Fig. 3(b), where a linear fit of the experimental data was implemented and an extremely high sensitivity of −9370.84 nm/RIU was obtained.

The linear response of the in-line single fiber MZI to the RI in a fine scale was also investigated by filling the cavity with water and varying its temperature. The temperature RI coefficient of the water is in the order of 10^{-4}/°C, much larger than that of fused silica (typically in the order of 10^{-5}/°C). Figure 4 demonstrates the wavelength shift of the device versus the RI change between 1.32770 and 1.33243, corresponding to the temperature

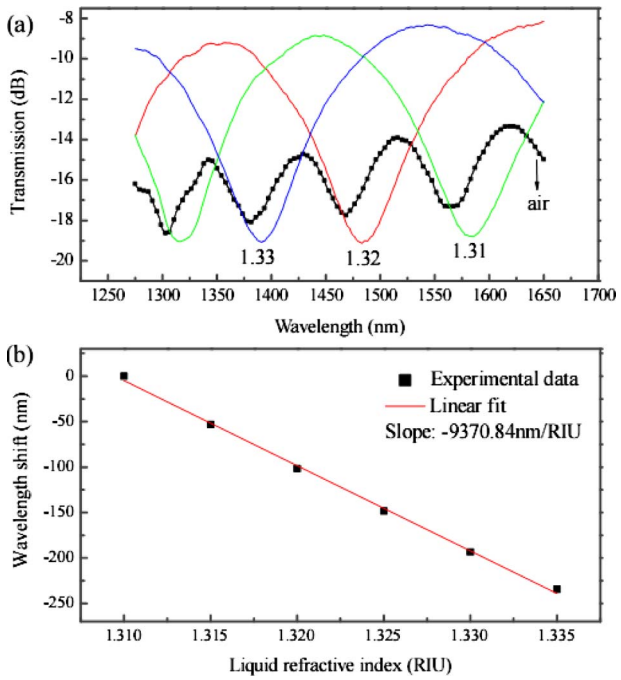

Fig. 3. (Color online) Interference spectra of the in-line fiber MZI. (a) Transmission spectra. (b) Wavelength shift versus the RI filled in the microcavity.

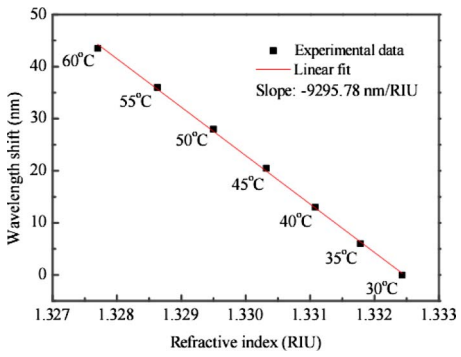

Fig. 4. (Color online) Wavelength shift of the in-line fiber MZI with water filled in the microcavity. Water temperature is varied between 30 and 60 °C.

variation from 60 to 30 °C [24]. A total wavelength shift of ~43 nm can be observed, and the RI sensitivity obtained is −9295.78 nm/RIU, which is in good agreement with the results obtained previously.

The essential difference between our MZI and those reported previously [10–16] lies in the fact that our device is based on the interference of the guided mode in the fiber core and the unguided mode travelling through the microcavity. The effective index difference between the two arms of the MZI is very large (>0.10), which allows a dramatic reduction of the cavity length while maintaining a high RI sensitivity. Moreover, the position of the RI change can be precisely located due to the small size of the microcavity.

Assuming that the cavity length is kept constant during the experiment, the sensitivity can be derived from Eq. (2) as

$$\frac{d\lambda}{d(\Delta n)} = \frac{\lambda}{\Delta n}. \tag{3}$$

This means that the sensitivity of an MZI device is determined by the effective index difference of the two interferometer arms in the microcavity and is independent of cavity length at precise wavelengths. According to Eq. (3), the sensitivity of the MZI developed in this work was calculated as 9924.1 nm/RIU at 1570 nm for $\Delta n = 1.4682 - 1.31 = 0.1582$, which is close to the experimental results obtained.

The FSR of the interference dip of interest is determined by the cavity length, L, as

$$\mathrm{FSR} = \frac{\lambda^2}{\Delta n L}, \tag{4}$$

which is determined by the OPD (ΔnL) of the two arms of the MZI device at a given wavelength. Taking the 51 μm cavity length as an example, the FSR around 1550 nm is approximately 105 and 362 nm for an air-filled cavity and a 1.32 RI liquid-filled cavity, respectively, which is in accordance with our experiments demonstrated in Fig. 3(a).

The detection limit (DL) can be determined with the smallest detectable change in resonance wavelength (R) and the sensitivity (S) by DL=R/S. White and Fan [25] have given a heuristic formula to estimate DL taking into account the signal-to-noise ratio (SNR), full width at half-maximum (FWHM) value of the resonance, thermal noise, and the OSA resolution. In our device, R is dominated by the FWHM value of the interference fringe, which is measured to be ~80 nm. Assuming a SNR of 50 dB, DL was calculated to be 3.0×10^{-4} RIU. DL could be further decreased by optimizing the interference fringe visibility of our MZI device, since the FWHM value of the fringe would be dramatically reduced with the increase of the fringe visibility.

The fiber in-line MZI developed would be attractive in optical fiber sensors owing to its simplicity, compactness, and extremely high sensitivity. Further efforts should be made to implement this structure in practical sensing applications. For instance, the cavity could be micromachined into a through-hole form to facilitate the liquid exchange in an optofluidic device, and the surface roughness of the cavity should be decreased to suppress the insertion loss of the device.

4. CONCLUSION

In conclusion, we have demonstrated a simple and compact fiber in-line MZI structure for RI measurement with extremely high sensitivity and precise sensing location. One arm of the MZI contains a microcavity created by femtosecond laser micromachining to remove part of the fiber core and cladding, and the other remains to be confined to the fiber core. The system has good operation linearity, and the sensitivity obtained is −9370 nm/RIU in the 1.31–1.335 RI range. Such a fiber device has high potential in chemical and biological sensor applications.

ACKNOWLEDGMENT

This work was supported by Hong Kong SAR government through a GRF (general research fund) grant PolyU 5306/08E.

REFERENCES

1. K. Shroeder, W. Ecke, R. Mueller, R. Willsch, and A. Andreev, "A fiber Bragg grating refractometer," Meas. Sci. Technol. **12**, 757–764 (2001).
2. W. Liang, Y. Huang, Y. Xu, R. K. Lee, and A. Yariv, "Highly sensitive fiber Bragg grating refractive index sensors," Appl. Phys. Lett. **86**, 151122 (2005).
3. K. Zhou, Y. Lai, X. Chen, K. Sugden, L. Zhang, and I. Bennion, "A refractometer based on a micro-slot in a fiber Bragg grating formed by chemically assisted femtosecond laser processing," Opt. Express **15**, 15848–15853 (2007).
4. V. Bhatia and A. M. Vengsarkar, "Optical fiber long-period grating sensors," Opt. Lett. **21**, 692–694 (1996).
5. D. W. Kin, Y. Zhang, K. L. Cooper, and A. Wang, "In-fiber reflection mode interferometer based on a long-period grating for external refractive-index measurement," Appl. Opt. **44**, 5368–5373 (2005).
6. D. W. Kim, F. Shen, X. Chen, and A. Wang, "Simultaneous measurement of refractive index and temperature based on a reflection-mode long-period grating and an intrinsic Fabry–Perot interferometer sensor," Opt. Lett. **30**, 3000–3002 (2005).
7. G. P. Agrawal, *Lightwave Technology: Components and Devices*, Wiley & Sons, 2004).
8. X. Fan, I. M. White, S. I. Shopova, H. Zhu, J. D. Suter, and Y. Sun, "Sensitive optical biosensors for unlabeled targets: A review," Anal. Chim. Acta **620**, 8–26 (2008).
9. R. Slavík, J. Homola, J. Čtyroky, and E. Brynda, "Novel spectral fiber optic sensor based on surface plasmon resonance," Sens. Actuators B **74**, 106–111 (2001).
10. V. P. Minkovich, J. Villatoro, D. Monzón-Hernández, S. Calixto, A. B. Sotsky, and L. I. Sotskaya, "Holey fiber tapers with resonance transmission for high-resolution refractive index sensing," Opt. Express **13**, 7609–7614 (2005).
11. B. H. Lee and J. Nishii, "Dependence of fringe spacing on the grating separation in a long-period fiber grating pair," Appl. Opt. **38**, 3450–3459 (1999).
12. J. H. Lim, H. S. Jang, K. S. Lee, J. C. Kim, and B. H. Lee, "Mach–Zehnder interferometer formed in a photonic crystal fiber based on a pair of long-period fiber gratings," Opt. Lett. **29**, 346–348 (2004).
13. H. Y. Choi, M. J. Kim, and B. H. Lee, "All-fiber Mach–Zehnder type interferometers formed in photonic crystal fiber," Opt. Express **15**, 5711–5720 (2007).
14. J. Villatoro, V. P. Minkovich, and D. Monzón-Hernández,

"Compact modal interferometer built with tapered microstructured optical fiber," IEEE Photon. Technol. Lett. **18**, 1258–1260 (2006).
15. Z. Tian, S. S.-H. Yam, J. Barnes, W. Bock, P. Greig, J. M. Fraser, H.-P. Loock, and R. D. Oleschuk, "Refractive index sensing with Mach–Zehnder interferometer based on concatenating two single-mode fiber tapers," IEEE Photon. Technol. Lett. **20**, 626–628 (2008).
16. P. Lu, L. Men, K. Sooley, and Q. Chen, "Tapered fiber Mach–Zehnder interferometer for simultaneous measurement of refractive index and temperature," Appl. Phys. Lett. **94**, 131110 (2009).
17. C. Grillet, P. Domachuk, V. Ta'eed, E. Mägi, J. A. Bolger, B. J. Eggleton, L. Rodd, and J. Cooper-White, "Compact tunable microfluidic interferometer," Opt. Express **12**, 5440–5447 (2004).
18. P. Domachuk, C. Grillet, V. Ta'eed, E. Mägi, J. Bolger, B. J. Eggleton, L. Rodd, and J. Cooper-White, "Microfluidic interferometer," Appl. Phys. Lett. **86**, 024103 (2005).
19. C. Monat, P. Domachuk, C. Grillet, M. Collins, B. J. Eggleton, M. Cronin-Golomb, S. Mutzenich, T. Mahmud, G. Rosengarten, and A. Mitchell, "Optofluidics: a novel generation of reconfigurable and adaptive compact architectures," Microfluid. Nanofluid. **4**, 81–95 (2008).
20. Y. Lai, K. Zhou, and I. Bennion, "Microchannels in conventional single-mode fibers," Opt. Lett. **31**, 2559–2661 (2006).
21. Y. Wang, D. N. Wang, M. Yang, W. Hong, and P. Lu, "Refractive index sensor based on a microhole in single-mode fiber created by the use of femtosecond laser micromachining," Opt. Lett. **34**, 3328–3330 (2009).
22. Y. J. Rao, M. Deng, D. W. Duan, X. C. Yang, T. Zhu, and G. H. Cheng, "Micro Fabry–Perot interferometers in silica fibers machined by femtosecond laser," Opt. Express **15**, 14123–14128 (2007).
23. T. Wei, Y. Han, Y. Li, H. L. Tsai, and H. Xiao, "Temperature-insensitive miniaturized fiber inline Fabry–Perot interferometer for highly sensitive refractive index measurement," Opt. Express **16**, 5764–5769 (2008).
24. P. Schiebener, J. Straub, J. M. H. Levelt Sengers, and J. S. Gallagher, "Refractive index of water and steam as function of wavelength, temperature and density," J. Phys. Chem. Ref. Data **19**, 677–717 (1990).
25. I. M. White and X. D. Fan, "On the performance quantification of resonant refractive index sensors," Opt. Express **16**, 1020–1028 (2008).